An Analytical Approach to Modeling Thin, Pre-Cracked Specimens Using Traction-Separation

A Proof of Concept

Adly, Mohammed A.; Walters, Carey L.

DOI
10.1115/OMAE2024-126655

Publication date
2024

Document Version
Final published version

Published in
Structures, Safety, and Reliability

Proceedings of the ASME 2024 43rd International Conference on Ocean, Offshore and Arctic Engineering
OMAE2024
June 9-14, 2024, Singapore, Singapore

OMAE2024-126655

AN ANALYTICAL APPROACH TO MODELING THIN, PRE-CRACKED SPECIMENS USING TRACTION-SEPARATION: A PROOF OF CONCEPT

Mohammed A. Adly[1], Carey L. Walters[1]

[1]Department of Maritime and Transport Technology
Faculty of Mechanical Engineering, Delft University of Technology
Delft, The Netherlands

ABSTRACT

Cohesive zone and eXtended Finite Element Modeling (xFEM) are promising methods for modeling the propagation of a crack using coarse meshes and hence saving considerable computational time. The Traction Separation Law (TSL) that is needed for such techniques is, however, mostly derived a posteriori using experiments. This prevents its widespread utilization in structures without high costs. For example, in the modeling of a compact tension test, the TSL is known to evolve as the crack grows. Qualitative physical explanations have been offered for this phenomenon. Necking ahead of the crack tip is thought to have a large effect on crack propagation, while the necking behavior in any given element is influenced by both the state of stress acting on it and the structural boundaries around it. However, a method to account for those explanations a priori in the TSL doesn't exist. Here, TSLs are developed for the elements along the known crack path in a middle crack tension test and implemented as a damage model in Abaqus. They are derived solely from the material properties and the element dimensions, thus excluding the need for inverse engineering based on experiments. This paves the way for more general applications of traction separation laws within the maritime and offshore industry.

Keywords: Traction Separation, Middle Crack Tension, Accidental Limit State, Fracture.

1. INTRODUCTION

Modelling crack propagation in thin-walled structures at the structural scale is necessary for the analysis of the safety of structures subjected to extreme loading in many industries including the maritime and offshore industries. The most common approach for analyzing the crack propagation in a given structure is using numerical techniques such as the Finite Element (FE) method. One of the principal issues with utilizing FE simulations to study crack propagation in engineering structures is the computational cost and time needed to obtain accurate results. This arises due to the fact that the driving physics of the crack and its propagation zone occur at a length scale that is orders of magnitude smaller than length scales of the full structure. While models used for the analysis of accidental limit state are typically carried out with shell elements that are about five times the element thickness [1], models used for the precise modelling of initiation and propagation of cracks are often created using solid elements that are a small fraction of the thickness. For example, in order to capture the ductile fracture in a Compact Tension (CT) test, the mesh resolution needs to be on the order of 100 µm [2]. Recently, some research was dedicated to trying to model pre-cracked specimens such as the CT and Middle Crack Tension (MCT) test using cohesive zone modelling and xFEM. In [3], physics-based TSLs were used to obtain more accurate results than conventional damage models. TSLs were also used for significantly reducing the number of needed elements in [4] but their parameters needed to be calibrated based on experimental results.

The work presented here attempts to bridge these two length scales by applying TSLs to achieve realistic simulations of crack propagation while maintaining shell element aspect ratios representative of full-scale ships. The traction-separation law (TSL) necessary for modelling of a MCT test with shell elements at this scale will be derived *a priori* using only the element sizes and the material model as inputs. It will be demonstrated in the results section that we are capable of predicting wholistic indicators of the test such as the maximum force and failure displacement within 10% of the experimental results and at a significantly reduced fraction of the computational effort and mesh density required to get similar results using the more conventional solid elements with the necessary dimensions.

This paper will therefore be organized as follows. Section two will introduce the experiment. Section three will offer the approach utilized to obtain the TSL. Section four will introduce the implementation method into a standard FE program. Section

five will contain the results. Section six will then offer the conclusions and the suggestions for future work.

2. MIDDLE CRACK TENSION (MCT) EXPERIMENT

The material used for manufacturing the specimens is a CSA G40.21 44W steel commonly used for maritime applications with a yield stress of approximately 350 MPa and a tensile strength of approximately 500 MPa. The material elasticity, plasticity and damage model are taken from a prior report [5]. Young's modulus is 186 GPa, and Poisson's ratio is 0.3. The plasticity model is a piecewise linear model with 82 points, and the damage model is Modified Mohr-Coulomb (MMC) [6] model calibrated using three different experiments to ensure that it is valid for a wide range of stress states. Those models are based on a von-Mises yield envelope with the associated flow rule. The damage model can be characterized by $c_1 = 0$ and $c_2 = 513$ MPa as presented in eq. (19) of [6] . The stress-strain diagram for the material is illustrated in Fig. 1.

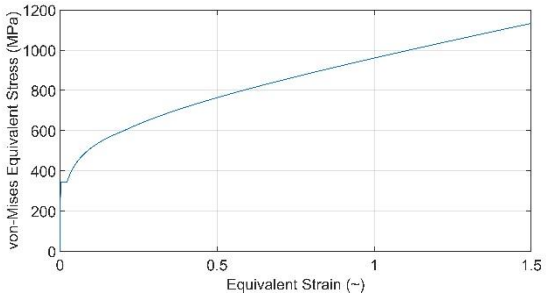

FIGURE 1: MATERIAL STRESS-STRAIN DIAGRAM

The geometry of the MCT specimen was based on ASTM E647-15 [7]. This resulted in the design shown in Fig. 2. The thickness of the base material was reduced from 5/16 inches (or about 8 mm) to obtain 2mm thick specimens.

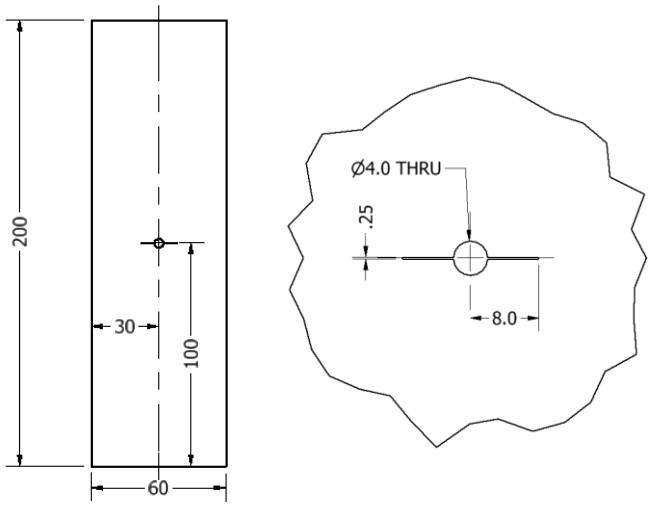

a b

FIGURE 2: MCT SPECIMEN: A) OVERVIEW, B) DETAILS, ALL DIMMENSIONS IN mm.

The cracks were manufactured with a wire Electrical Discharge Machining (EDM), and they were not fatigue sharpened. Three samples of this specimen geometry were manufactured to verify the consistency of test results. The specimens were spray painted on one side to allow for use of Digital Image Correlation (DIC) to measure displacements. The specimens were gripped between the upper moving jaw and lower stationary jaw of a 250 kN Instron tension testing machine. The experimental setup is illustrated in Fig. 3.

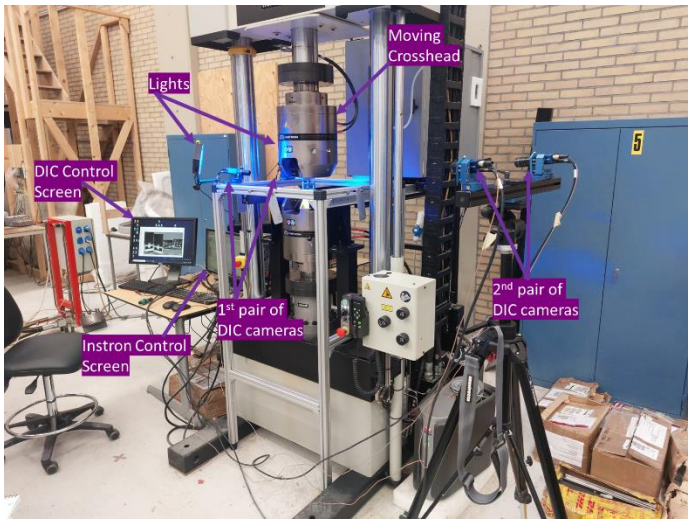

FIGURE 3: EXPERIMENTAL SETUP

Two pairs of DIC cameras were utilized where one pair photographed the painted side of the specimen while the second photographed the unpainted back side to be better able to monitor the crack progression without the paint obstructing the view. The tests were conducted with a displacement speed of 1 mm/min. A typical specimen is shown in Fig. 4 both before performing the experiment and with a fully developed crack afterwards.

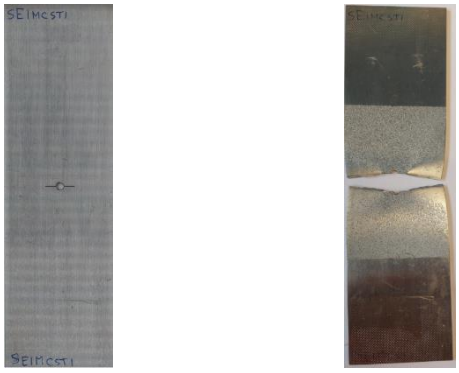

a b

FIGURE 4: MANUFACTURED MCT SPECIMEN: A) PRE EXPERIMENT, B) WITH A FULLY DEVELOPED CRACK AFTER THE EXPERIMENT

3. ANALYTICALLY DERIVED TSL

It will be assumed during the TSL development that strips across the thickness of the MCT specimen ahead of the crack can be approximated as in Fig. 5.

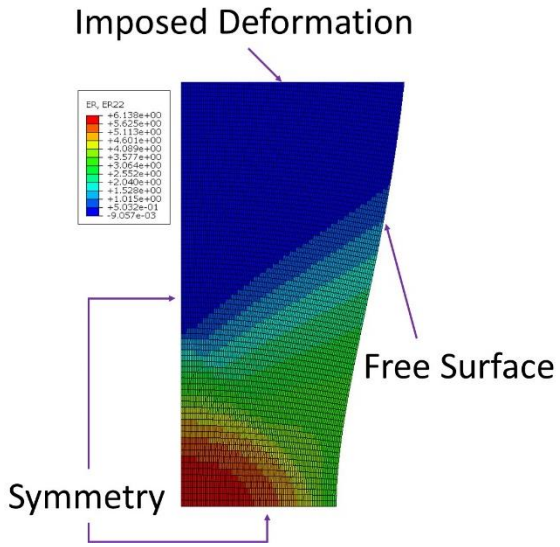

FIGURE 5: LOCALIZING SEGMENT OF A PLANE STRAIN SPECIMEN IN TENSION; COLORS INDICATE THE STRAIN RATE IN THE VERTICAL DIRECTION WITH BLUE SIGNIFYING ELASTIC UNLOADING

The horizontal dimension in Fig. 5 therefore denotes the thickness of the MCT specimen while the vertical dimension is the same. Each cross section in the thickness direction of the MCT specimen at various distances from the crack tip will be assumed to be a plane strain section undergoing tension.

Even though both of those assumptions would be considered as an approximation rather than a reflection of the true physical reality, it is thought that they wouldn't significantly affect the validity of the adopted method. This will be discussed in the results section.

The use of a TSL offers advantages when applied with large elements. It will help to enable mesh objectivity by accounting for phenomena that are small relative to the size of elements that larger ship and offshore structures can be meshed with. This is because an advancing crack generates acute stress fields at the crack tip and can induce necking (which has a length on the order of the thickness) that may be smaller than elements that are used to model full structures are able to capture. Not accounting for these local effects would lead to the crack propagation being excessively delayed in case the same failure model is used as with the finer scaled elements. The TSL therefore acts as a way to analytically predict the effects at the point of stress and strain concentration and relate it to the displacements and behavior of a much larger element. In this section, an analytical approach for estimating TSL's is derived based on an approximation of localizations that are occurring on the scale of the material thickness. The general overview of this method is given in Fig. 6, and the theory is outlined in the remainder of this section.

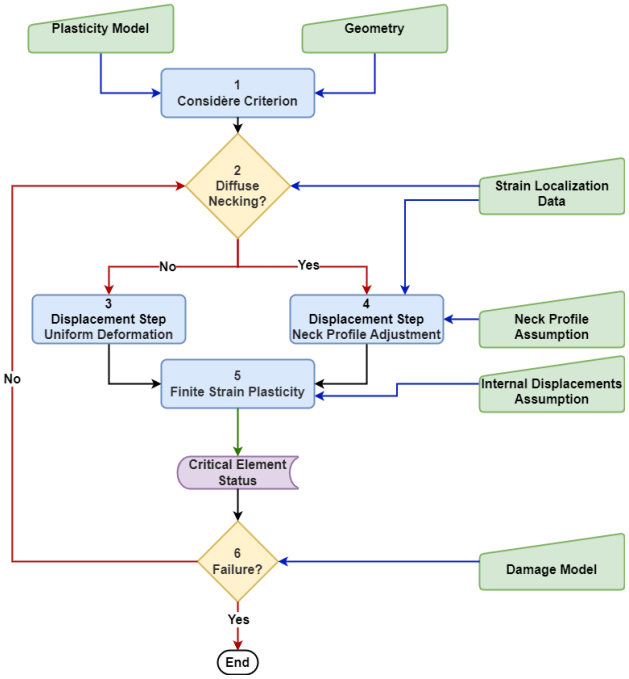

FIGURE 6: TSL METHODOLOGY

The divergence between the behavior of small element and that of a bigger element in a relatively homogenous stress field only starts occurring once localization starts manifesting itself in the structure. Therefore, the multi-scale coupling of the behavior at a finer scale with that at a larger scale is only necessary post localization initiation. The starting point for the analytical model is therefore the earliest possible point for localization, which can be signaled by the Considère criterion [8] in block 1 where the maximum of an engineering stress-strain curve would occur. This is informed by the hardening model relating the equivalent strains and stresses and the geometry of the structure.

In block 2, it is decided if localization starts occurring at exactly the maximum point of an engineering stress-stain curve or is further delayed. Other factors, such as the bifurcation tendency of the structure based on its dimensions and the element size would have an influence on that [9]. Once the neck is formed, plastic deformation starts concentrating in an area closer to the center of the specimen and totally stops outside of a certain region. The material outside this region then starts to unload elastically. This can be seen in Fig. 5 where the deep blue zone indicates the region with negative vertical strain rates. The extent of this actively plastically deforming zone decreases with the development of the neck and we have observed it to be related to the current minimum neck thickness. This correlation is then used to indicate if localization has already initiated in the structure or not based on its current dimensions. The successive iterative displacement steps are therefore either assuming uniform deformation or a curvature in the neck profile.

In case of no localization initiation, a uniform deformation occurs in the structure as in block 3 of Fig. 6. This simply denotes the elongation of the structure with the accompanying uniform

contraction in the horizontal dimension to maintain constant volume. In case localization is indicated to have initiated, diffuse necking is simulated in the structure in block 4 of Fig. 6. Diffuse necking is simulated by adjusting the neck profile where it is assumed to follow a developing third order polynomial at the deepest part of the neck where it is always vertical at the deepest part of the neck and maintaining the slope at the freezing point at the interface between the plastically deforming zone and the elastically unloading zone.

In block 5 of Fig. 6, the principles of finite strain plasticity are used to estimate the strain at the critical point of the structure at the intersection of the vertical and horizontal symmetry planes. In order to use finite strain plasticity, a displacement field needs to be known for the structure. This displacement field is obtained through two assumptions. First, the position of the initially vertical lines within the structure are assumed to remain proportional to the displacement of the outer profile of the neck following the assumption of Bridgman [10]. Second, the initially horizontal lines anywhere in the material are assumed to deform forming a second order polynomial which is horizontal at the vertical symmetry plane and perpendicular to the neck profile at its edge. Through applying those two considerations, the displacement field can then be known, and it is possible to calculate the strains. The strain components at the critical point are then converted to stress components through the plasticity model and knowing the boundary stresses of the structure at the outer profile of the neck.

Finally, a model is needed to indicate when failure would occur at the critical point. This is indicated by block 6 in Fig. 6. A failure model such as the Modified Mohr Coulomb (MMC) [6] (or others) can then be applied to ascertain if local failure occurs at this point or not. This leads to the linking of the local failure criterion with the global displacement behavior of the structure. The global displacement of an element from the earliest possible moment of localization initiation untill the moment of failure at its most critical point can then be deduced and utilized for the FE implementation of this TSL.

4. FE IMPLEMENTATION

Two finite element simulations were undertaken in order to capture the behavior of the MCT experiment. The first simulation used solid elements of sufficiently fine dimensions to capture the crack propagation behavior based on element erosion techniques and MMC theory alone. The second simulation was done using shell elements of target element size four times the thickness of the specimen (approximately 64 times the dimension of the smallest solid elements) in order to demonstrate the use of TSLs in crack propagation simulations for shell elements that are representative of simulations for accidental limit states. All of the simulations were carried out using the dynamic explicit solver in Abaqus 2021.HF5 [11].

4.1 Solid Simulation

The first simulation used solid elements of the type C3D8R, which is a general purpose 8 noded brick element with reduced integration. As is common with solid element FE simulations of cracked specimens, 10 elements spanned the crack opening, and 16 elements spanned the thickness. This is considered the resolution necessary in order to properly capture the stresses ahead of a crack and its propagation. The mesh in the vicinity of the crack is shown in Fig. 7.

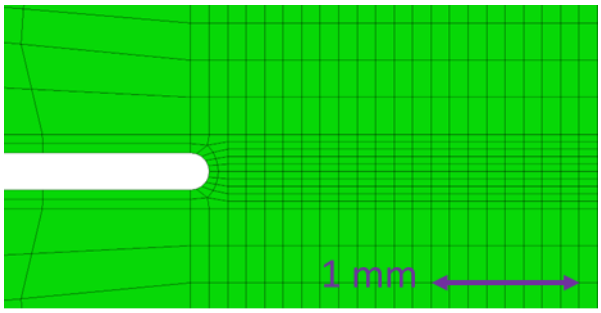

FIGURE 7: MESH IN THE VICINITY OF THE CRACK IN THE SOLID SIMULATION

The mesh represented one vertical half of the specimen, which accounted for the symmetry condition at its vertical symmetry plane and only covers a portion 40 mm below and above the crack. This was the portion of the specimen not covered by the grips. The displacement at a point at the vertical symmetry line of the specimen and 30 mm above the center is chosen to be the measurement point from the DIC analysis of the experiment to be compared with the same point in the simulation. Symmetry in the horizontal plane or thickness directions was not imposed in order to capture shear banding. The simulated portion of the structure along with a bigger overview of the mesh are shown in Fig. 8.

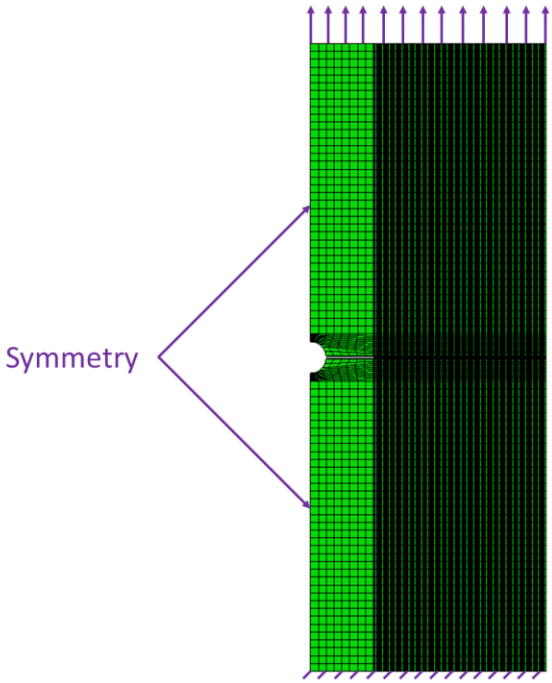

FIGURE 8: SOLID SIMULATION SPAN AND MESH

This arrangement resulted into a mesh of 311168 elements across the simulated span. In addition to applying symmetry at the vertical symmetry plane, the lower edge was fixed to simulate being in the stationary grip and the upper edge was given a vertical velocity 1 mm/min while being fixed in all the other degrees of freedom. No strain rate effects were considered in either the plasticity or the damage model due to this being a quasi-static simulation. Element deletion was employed the moment failure conditions were met according to the MMC damage model. A total simulation time of 420 s was chosen, as this corresponds to a time slightly longer than that was needed until total fracture during the experiment. A semi-automatic mass scaling regime was employed in order to keep the timestep greater than 10^{-4} s. When compared with the results produced using a mass scaling regime to keep the timestep only greater than 10^{-3} s, the maximum forces were within 1% of each other while the displacement at complete fracture was 4% more than in the condition with more mass scaling. This implies that the simulation was not sufficiently convergent regarding the post maximum force performance, but it was infeasible to further reduce the mass scaling with the available computational resources. With the current conditions, this simulation took 128 hours on a 3.60 GHz Intel Xeon W-2233 CPU with 16 GB of RAM. The mesh in the vicinity of the crack at the end of the simulation is shown in Fig. 9.

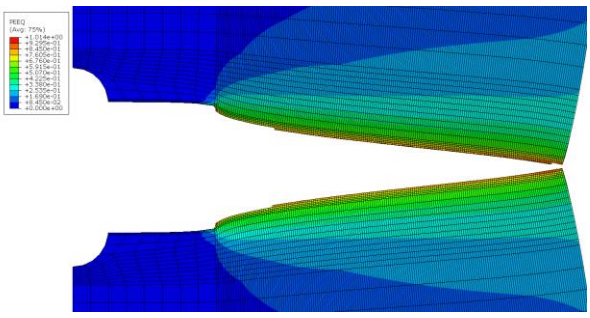

FIGURE 9: SOLID SIMULATION MESH POST FRACTURE IN THE VICINITY OF THE CRACK. COLORS DENOTE EFFECTIVE PLASTIC STRAIN.

4.2 Shell Simulation

Many factors had to be considered in order to properly apply the developed TSL in a shell simulation with elements as big as previously mentioned. This starts with the mesh in the vicinity of the crack tip, which is shown in Fig. 10.

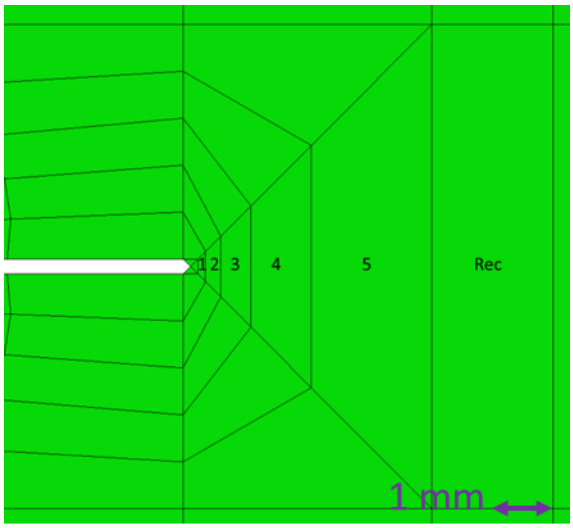

FIGURE 10: MESH IN CRACK TIP VICINITY IN SHELL SIMULATION

First, the semicircular crack tip was replaced with a triangular crack tip. This was to facilitate in the creation of the successive gradually growing elements. Three triangular elements of the type S3R (triangular 3 noded shell elements with reduced integration) were created at the immediate vicinity of the crack. All the other elements in the structure were of the type S4R (4 noded shell elements with reduced integration). The 3 triangular elements, the trapezoidal elements numbered one through 5 and the rectangular elements in the direction of the crack extension all had specific damage models incorporating the TSLs developed according to Section 3. Rather than creating dedicated Cohesive Elements, the TSLs were implemented into Abaqus as modified ductile failure material properties. This means that the traction-separation relationship is incorporated in Abaqus as a gradual loss of the tractional capacity of the element (damage evolution) correlated to the deduced displacement from the moment of damage initiation to the moment of fracture of the element from section three. Each of the elements discussed above therefore had an identical material model definition in Abaqus but a different damage model was incorporated for each of them based on how the different element dimensions affected the displacement from damage initiation to fracture as informed from section three.

The damage initiation parameter for each of those elements was decided to be at an equivalent plastic strain at initiation $\bar{\varepsilon}_i = 0.23$. This corresponds to the earliest possible point of localization initiation according to [8] for the utilized material model and corresponds with the TSL initiation point previously discussed in section three. For the three triangular elements immediately at the tip of the crack, this value was chosen to also represent instant fracture upon initiation due to the expected stress concentrations at this point. Once the rectangular element is gradually reached, the same element size continues until the end of the specimen. The rest of the structure was modelled using normal shell elements. The whole mesh can be seen in Fig. 11.

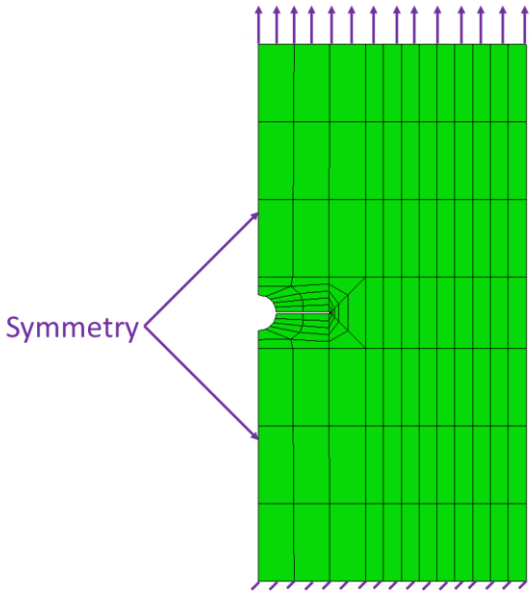

FIGURE 11: SHELL SIMULATION SPAN AND MESH

This meshing strategy was chosen for a variety of reasons. First, in the vicinity of the crack tip, small element sizes are needed just to capture the initial stress concentration and geometry. Second, it is desired to use elements as big as possible (4 times the thickness) in order to more closely represent accidental limit state simulations done on large structures or sections thereof. Third, the transition between the small mesh size and the larger one has to be gradual. Finally, it was not desired to have a very large element dimension in the direction of the crack propagation in order to have some smoothness in the results with the presence of element deletion. It is due to this final constraint that the element dimension in this direction was limited to 2 mm.

Table 1 will offer some of the relevant properties and the displacement of the successive elements from the moment of damage initiation (earliest possible localization initiation) till complete fracture along the crack propagation direction as calculated using the TSLs. The average length of each element is denoted as L_{avg}; its area is denoted as A; and the vertical displacement from damage initiation to fracture is denoted as d_f.

TABLE 1: ELEMENT PROPERTIES AND FAILUIRE DISPLACEMENT

Element	L_{avg} [mm]	A [mm^2]	d_f [mm]
Trapezoid 1	0.375	0.047	0.3
Trapezoid 2	0.75	0.189	0.58
Trapezoid 3	1.5	0.75	0.92
Trapezoid 4	3	3	0.98
Trapezoid 5	6	12	0.78
Rectangular	8	16	0.78

While implementing the TSL, it was chosen to implement a linear damage model to reflect the fact that the load carrying capacity across the width of an element decreases gradually as the crack propagates through it. This means that the damage parameter D changes from a value of 0 at damage initiation to a value of 1 at total fracture (corresponding to the vertical displacement at failure) in a linear manner. The effect of the damage parameter on the load carrying capacity of an element is shown in eq. (1) [11].

$$\overline{\sigma_d} = (1 - \mathrm{D})\bar{\sigma} \tag{1}$$

Here, $\bar{\sigma}$ is the equivalent stress of an element, and $\overline{\sigma_d}$ is the equivalent stress of the element post damage initiation. The difference between them is the loss of tractional (load carrying) capacity of the element post damage initiation. The vertical displacement at fracture also needs to be converted to an effective plastic displacement at fracture u_f for utilization in Abaqus [11]. This simply signifies the change in the equivalent plastic strain of an element from the moment of damage initiation to the moment of total fracture but related through the characteristic length of the element. The vertical length of an element at the moment of damage initiation is noted as L_n, and therefore the vertical strain ε_{vf} at failure can be calculated as in eq. (2).

$$\varepsilon_{vf} = \ln\frac{L_n + d_f}{L_{avg}} \tag{2}$$

Due to the assumption that the cross sectional strips of the specimen in the thickness direction can be approximated as plane strain blocks in tension, the strain in the direction of the width of the specimen can be considered to be 0 and the equivalent plastic strain at failure $\bar{\varepsilon_f}$ can therefore be related to its vertical strain as in eq. (3).

$$\bar{\varepsilon_f} = \sqrt{\frac{2}{3}}\varepsilon_{vf} \tag{3}$$

The change in equivalent plastic strain between damage initiation and complete fracture can then be calculated as in eq. (4).

$$\Delta\bar{\varepsilon} = \bar{\varepsilon_f} - \bar{\varepsilon_i} \tag{4}$$

The characteristic length of each element L_c for quadratic elements with reduced integration is the square root of the area, as shown in eq. (5).

$$L_c = \sqrt{A} \tag{5}$$

The value needed for the damage evolution model in Abaqus and named as the effective plastic displacement at fracture u_f [11] can therefore be calculated as in eq. (6).

$$u_f = \bar{\varepsilon_f} * L_c \quad (6)$$

All the necessary inputs for the chosen damage evolution model in all the elements in Abaqus are therefore present. The damage variable D at any instance post damage initiation can therefore be correlated to its current effective plastic displacement u according to eq. (7).

$$D = 1 - \frac{u_f - u}{u_f} \quad (7)$$

The damage progression for each element along the crack extension direction against its effective plastic displacement is therefore shown in Fig. 12 and the loss in tractional capacity can be described using eq. (1)

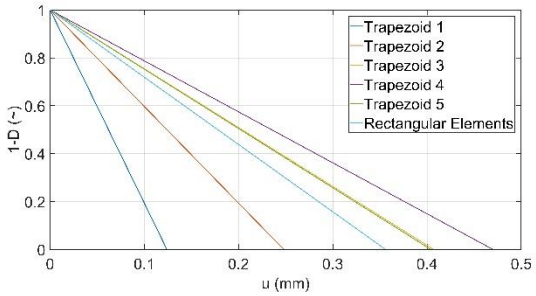

FIGURE 12: DAMAGE MODELS FOR DIFFERENT ELEMENTS

The whole mesh in Fig. 11 consists of 121 elements across the simulated span. The same boundary conditions, simulation time and mass scaling strategies as the solid simulation were used. Here, element deletion was applied at the moment that D reaches a value of 1 in any of the elements along the crack path. With those alterations, the simulation took about 20min on a 1.70 GHz Intel Core i5 CPU with 8 GB of RAM. The mesh in the vicinity of the crack at the end of the simulation is shown in Fig. 13.

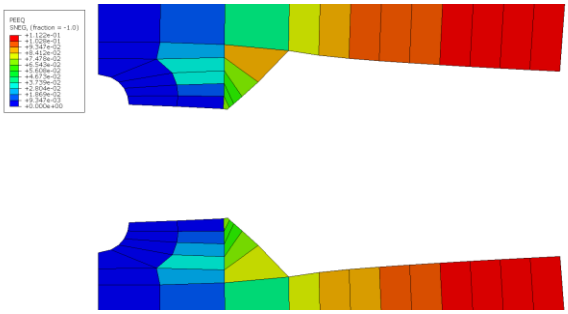

FIGURE 13: SHELL SIMULATION MESH POST FRACTURE IN THE VICINITY OF THE CRACK, COLORS DENOTE EFFECTIVE PLASTIC STRAIN

5. RESULTS AND DISCUSSION

The force-displacement diagram containing the experimental results and the FE results from both the solid simulation and the shell simulation is shown in Fig. 14.

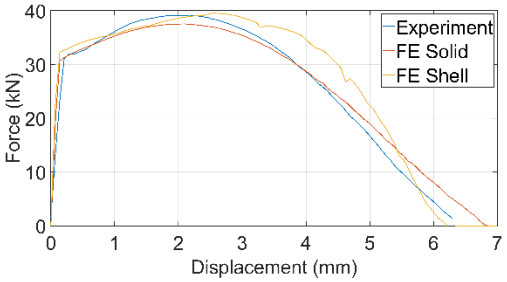

FIGURE 14: FORCE-DISPLACEMENT DIAGRAM

The values for the maximum force F_{max} and displacement at fracture d_{fra} (due to the noise in the experimental measurements, this will be taken at the point at which a force of 1 kN is reached) for the experiment and both simulations will be highlighted in Table 2. The error indicates the absolute percentage difference between a simulation result and the experimental result.

TABLE 2: KEY RESULT PARAMETERS

	Experiment	Solid FE	Shell FE
F_{max} [kN] (Error - %)	39.2	37.6 (4.1%)	39.5 (0.1%)
d_{fra} [mm] (Error - %)	6.37	6.72 (5.5%)	6.16 (3.3%)

First, some observations need to be addressed regarding the solid simulation as this should exhibit high accuracy with regards to matching the experiment. The error in the elastic portion of the simulation making the simulation significantly stiffer than the experiment is thought to be related to the elastic material model. Second, although the error in the maximum force is within 5% of the experimental result, this can be improved with a better material and damage model. Finally, the variation between the simulation and the experiment post maximum force can be improved by reducing the mass scaling; that was not feasible with the available computational capabilities.

Several observations need to be mentioned regarding the shell simulation results, which are the main contribution of this paper. The periodic dips of the force curve can be attributed to the coarse mesh leading to element deletion causing some jumps in the load carrying capacity. This is, however, much better than traditional element erosion techniques. However, the utilization of this approach would be highly valuable in obtaining a sufficiently accurate estimate of the wholistic performance of a cracked specimen simulation at a significantly reduced computational effort. The errors in the maximum force and displacement at fracture were predicted to be within 5% of the experimental results with a much coarser mesh (121 elements instead of 311168) and significantly less computational time (20

minutes instead of 128 hours). Even though the results show qualitatively similar behavior and key results are similar, the correlation throughout the curve after the maximum force is not as good as the solid simulation. This highlights the need for improvements to the current approach before it can produce higher fidelity results.

This study has therefore provided a method where crack propagation from a blunted or advancing crack can be modeled on a very large length scale, with a mesh density that is commensurate with full ship simulations. Much progress has been made, addressing many of the problems typically associated with more typical methods. There are nevertheless important differences between the simple case considered in this study, such as the possibility of advancing of mixed-mode cracks or states of stress that include multi-axial tension. More research is needed on more complex scenarios and improving the correlation.

6. CONCLUSION

An approach for the development and utilization of TSLs in the simulation of pre-cracked specimen experiments has been presented in this paper. TSLs were utilized with shell elements on a scale commensurate with that regularly used in full ship simulations. It is notable that this mesh was able to achieve predictions with the associated errors within 5% for the maximum force and fracture displacement. This shows the potential of the use of TSLs in the simulation of experiments involving propagating cracks, which conventionally require extremely fine meshes. Potential areas for improvement include:

- Incorporating the effect of the different stress states that could be affecting the various elements (permitting the study of the problem without assuming that a state of plane strain tension sufficiently captures the behavior of all elements ahead of the crack tip).
- Including the effects of varying strain rates.
- Studying the possible effects of varying the width of various elements alongside the crack propagation direction.

Further research would be needed to account for advancing mixed-mode cracks or stress states such as multi-axial tension.

ACKNOWLEDGEMENTS

This work has been done within the FailSafeShip project funded by the Dutch Research Council (NWO grant 17112) and with significant contributions from the Netherlands Organization for Applied Scientific Research (TNO), Femto Engineering and Commando Materieel en IT (COMMIT), Nederlandse Ministerie van Defensie to which we are all highly grateful for their contributions. We would also like to thank Maarten Korving, a TU Delft Master Student working alongside Femto Engineering for his insights towards Abaqus Implementation.

REFERENCES

[1] “Determination of Structural Capacity by Non-Linear FE Analysis Methods.” DNV-RP-C208. Det Norske Veritas AS. 2013.

[2] Nielsen, Kim Lau and Hutchinson, John W. “Cohesive Traction-Separation Laws for Tearing of Ductile Metal Plates.” International Journal of Impact Engineering Vol. 48 (2012): pp. 15-23. DOI 10.1016/j.ijimpeng.2011.02.009.

[3] Sidharth, Rajeev, Nikhil, R., Krishnan, S.A., Keralavarma, Shyam M., Moitra, Aniruddha and Vasudevan, M. “Crack Initiation and Growth in 316LN Stainless Steel: Experiments and XFEM Simulations.” Engineering Fracture Mechanics Vol. 274 (2022): pp. 108770. DOI 10.1016/j.engfracmech.2022.108770.

[4] Woelke, Pawel, Shields, Michael D. and Hutchinson, John W. “Cohesive Zone Modeling and Calibration for Mode I Tearing of Large Ductile Plates.” Engineering Fracture Mechanics Vol. 147 (2015): pp. 293-305. DOI 10.1016/j.engfracmech.2015.03.015.

[5] Roussel, Lucie. “Ductile fracture prediction of CSA G40.21 44W steel based on Modified Mohr-Coulomb model.” Delft University of Technology, Delft, The Netherlands. 2021.

[6] Bai, Yuanli and Wierzbicki, Tomasz. “Application of Extended Mohr-Coulomb Criterion to Ductile Fracture.” International Journal of Fracture Vol. 161 (2010): pp. 1-20. DOI 10.1007/s10704-009-9422-8.

[7] “Standard Test Method for Measurement of Fatigue Crack Growth Rates.” E647 – 15. ASTM International, West Conshohocken, Pennsylvania. 2015.

[8] Considère, Armand G. Memoire sur l’emploi du fer et de l’acier dans les constructions. Annales des Ponts et Chausses. (1885).

[9] Audoly, Basile and Hutchinson, John W. “Analysis of Necking Based on a One-Dimensional Model.” Journal of the Mechanics and Physics of Solids Vol. 97 (2016): pp. 68-91. DOI 10.1016/j.jmps.2015.12.018.

[10] Bridgman, Percy Williams. Studies in Large Plastic Flow and Fracture. Harvard University Press, Cambridge, Massachusetts (1952).

[11] “Abaqus 2021 User Manual.” Dassault Systems Simulia. 2021.

